LANGMUIR

pubs.acs.org/Langmuir Article

Anisotropic Compartmentalization of the Liquid–Liquid Interface using Dynamic Imine Chemistry

Chinmayee Agashe, Rohit Varshney, Rekha Sangwan, Arshdeep K. Gill, Mujeeb Alam, and Debabrata Patra*

Cite This: *Langmuir* 2022, 38, 8296–8303 Read Online

ACCESS | Metrics & More | Article Recommendations | Supporting Information

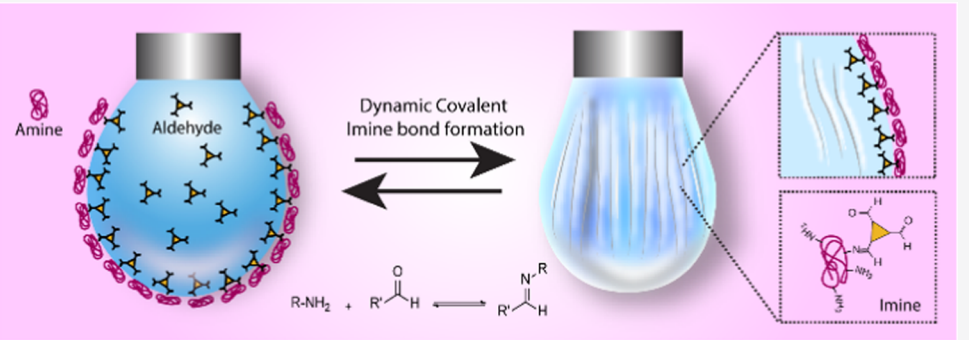

ABSTRACT: The liquid–liquid interface offers a fascinating avenue for generating hierarchical compartments. Herein, the dynamic imine chemistry is employed at the oil–water interface to investigate the effect of dynamic covalent bonds for modulating the droplet shape. The imine bond formation between oil-soluble aromatic aldehydes and water-soluble polyethyleneimine greatly stabilized the oil–water interface by substantially lowering the interfacial tension. The successful jamming of imine-mediated assemblies was observed when a compressive force was applied to the droplet. Thus, the anisotropic compartmentalization of the liquid–liquid interface was created, and it was later altered by changing the pH of the surrounding environment. Finally, a proof-of-concept demonstration of a pH-triggered cargo release across the interfacial membrane confirmed the feasibility of stimuli-responsive behavior of dynamic imine assemblies.

1. INTRODUCTION

The temporal and spatial sculpting of liquids has garnered interest in designing a nonequilibrium system for possible applications in catalysis, energy conversion, three-dimensional (3D) printing, and soft robotics.[1−5] The liquid–liquid interface offers a fascinating avenue for generating such architectures that can be reversibly modulated after fabrication.[6,7] The basis of the liquid–liquid interfacial interaction is the reaction between individual components of the two phases.[8,9] Such interactions result in an overall reduction of interfacial tension between the two liquids due to the formation of a two-dimensional (2D) network at the interface. Once the assemblies are formed, the interface can be transformed into various nonequilibrium structures.[10,11] These structured liquids can hold their nonequilibrium shape indefinitely when the interface is compressed.[12] In recent years, noncovalent supramolecular interactions such as hydrogen bonding,[13] electrostatic,[14,15] charge transfer,[16] and host–guest interactions[17] have been utilized to structure the liquid–liquid interface. The inherent dynamic and reversible nature of supramolecular interactions allowed the integration of stimuli-responsive behaviors into the interfacial assemblies. However, these assemblies are fragile and susceptible to solvent polarity, ionic strength, and temperature, thus limiting their applications for robust usage such as all-liquid 3D printing.

In this context, dynamic covalent chemistry can provide a complementary approach, which integrates the advantages of both covalent and noncovalent bonds. The dynamic covalent bond is robust yet can be reversibly modulated to create stimuli-responsive assemblies and numerous functional materials.[18] One of the most promising reactions under the umbrella of dynamic covalent bond is imine bond formation between an aldehyde and an amine. It is a reversible reaction that operates under thermodynamic control. For this fundamental reason, the dynamic imine bond has been successfully used for constructing molecular cages,[19] emulsions,[20,21] synthetic protocells,[22] stimuli-responsive polymers,[23] functional

Received: March 22, 2022
Revised: June 14, 2022
Published: June 28, 2022

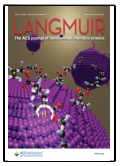

https://doi.org/10.1021/acs.langmuir.2c00725
Langmuir 2022, 38, 8296–8303

Scheme 1. Chemical Structures and Imine Reaction of PEI and Aldehydes

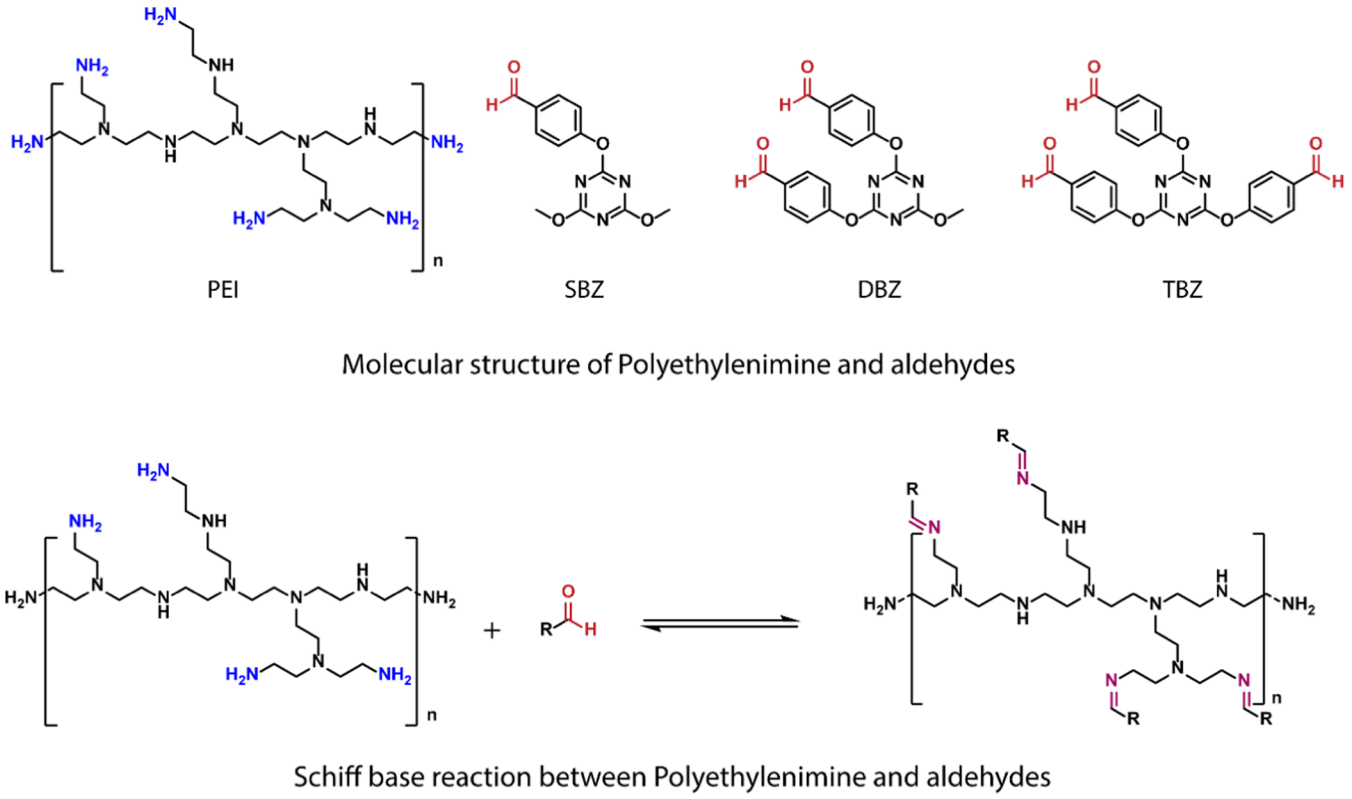

COFs,[24,25] motor,[26] micelles,[27] vesicles,[28,29] and functional coatings.[30,31]

Despite the enormous utilization of imine bond chemistry for the fabrication and modulation of functional assemblies, there has been limited focus on its application for liquid−liquid interfacial assemblies. It prompted us to investigate the use of multifaceted dynamic covalent imine bonds to structure liquids at the interface.

In this study, oil-soluble aromatic aldehydes and water-soluble polyethylenimine were used as biphasic components to construct imine-mediated assemblies at the oil−water interface. The formation of imine bonds markedly reduced the interfacial tension, and it was further tuned by varying the degree of aldehyde (mono, di, tri) functionality on the imine bond formation. The anisotropic compartmentalization of the liquid droplet was achieved by jamming the imine-mediated assemblies at the interface, and the dynamic nature of imine chemistry was utilized to further modulate the jamming to unjamming transition at the droplet interface. Finally, the imine bond-mediated assemblies provided a pH-responsive molecular transport across the droplet membrane.

2. RESULTS AND DISCUSSION

Water-soluble branched polyethylenimine (PEI) and organic soluble small molecule aldehydes were used to form imine-based assemblies at the oil−water interface. A series of aromatic aldehydes with a varying number of aldehyde groups were synthesized, namely, 4,4′,4″-((1,3,5-triazine-2,4,6-triyl)-tris(oxy))tribenzaldehyde, 4,4′-((6-methoxy-1,3,5-triazine-2,4-diyl)bis(oxy))dibenzaldehyde, and 4-((4,6-dimethoxy-1,3,5-triazin-2-yl)oxy)benzaldehyde, following the procedure reported in the literature (see the Supporting Information, Schemes S1−S3), and were termed as TBZ, DBZ, and SBZ, respectively, as shown in Scheme 1. The characterization of these compounds, such as ^{1}H, ^{13}C NMR, and IR, is provided in the Supporting Information Figures S1−S9. To assess the interfacial activity of the aldehydes and PEI, a stock solution of 1.0 mg/mL aldehydes in 1,2-dichlorobenzene (DCB) and 1% w/w aqueous solution of PEI were prepared. The dynamic interfacial tension was measured using a pendant drop tensiometer where a oil-soluble aldehyde drop was suspended in an aqueous solution of PEI, and the interfacial tension was monitored until the equilibrium was achieved.

In the first experiment, the PEI/TBZ pair was used to monitor the interfacial imine formation. The interfacial tension of TBZ/DCB was found to be ≈34.6 mN/m, which was close to the interfacial tension of the DCB/water system (37.2 mN/m). It indicated that TBZ has a minimum effect in stabilizing the oil−water interface. In the case of PEI/DCB, the equilibrium interfacial tension was reduced to 22 mN/m, and the reduction in interfacial tension could possibly be due to the electrostatic interaction between the positively charged PEI and the negatively charged oil−water interface.[32] The next measurement was carried out with the PEI/TBZ system, and the interfacial tension was markedly reduced to 11 mN/m. This observation clearly hinted toward the formation of stable conjugates, i.e., imine bond formation at the interface. To investigate the chemical functionalities presented in the interfacial film, ATR-IR spectroscopy analysis was performed by collecting a small fragment of the film on a silicon substrate (see the Supporting Information, Figure S10).

It revealed that the N−H stretching peaks of the primary amine in PEI at 3278 and 3340 cm^{-1} and a sharp peak of aldehyde carbonyl at 1700 cm^{-1} were greatly diminished in the interfacial film. The appearance of a new carbonyl peak at 1753 cm^{-1} confirmed the formation of an imine bond at the

https://doi.org/10.1021/acs.langmuir.2c00725
Langmuir 2022, 38, 8296−8303

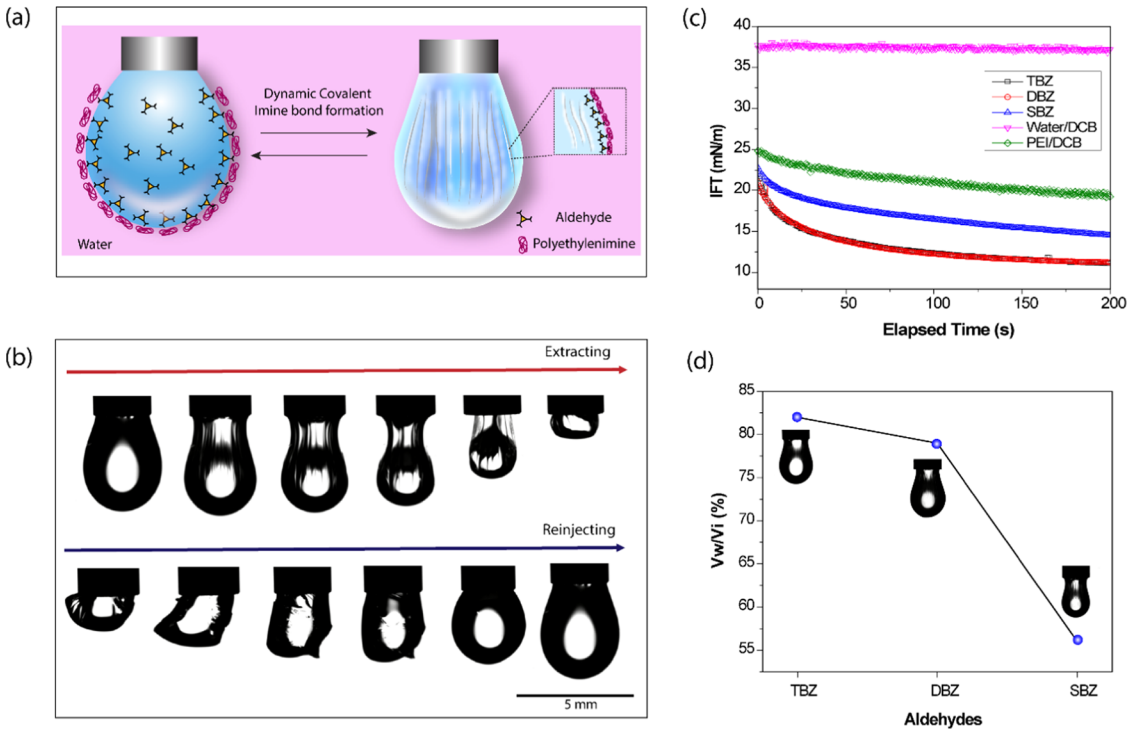

Figure 1. (a) Schematic representation of jamming due to imine bond formation at the interface. (b) Snapshots showing droplet morphology during extraction and reinjection (TBZ = 1.0 mg/mL, PEI 1% w/w). (c) Time evolution of interfacial tension. (d) Equilibrium IFT and surface coverage with PEI (1% w/w) and a series of aldehydes, TBZ, DBZ, and SBZ (1.0 mg/mL).

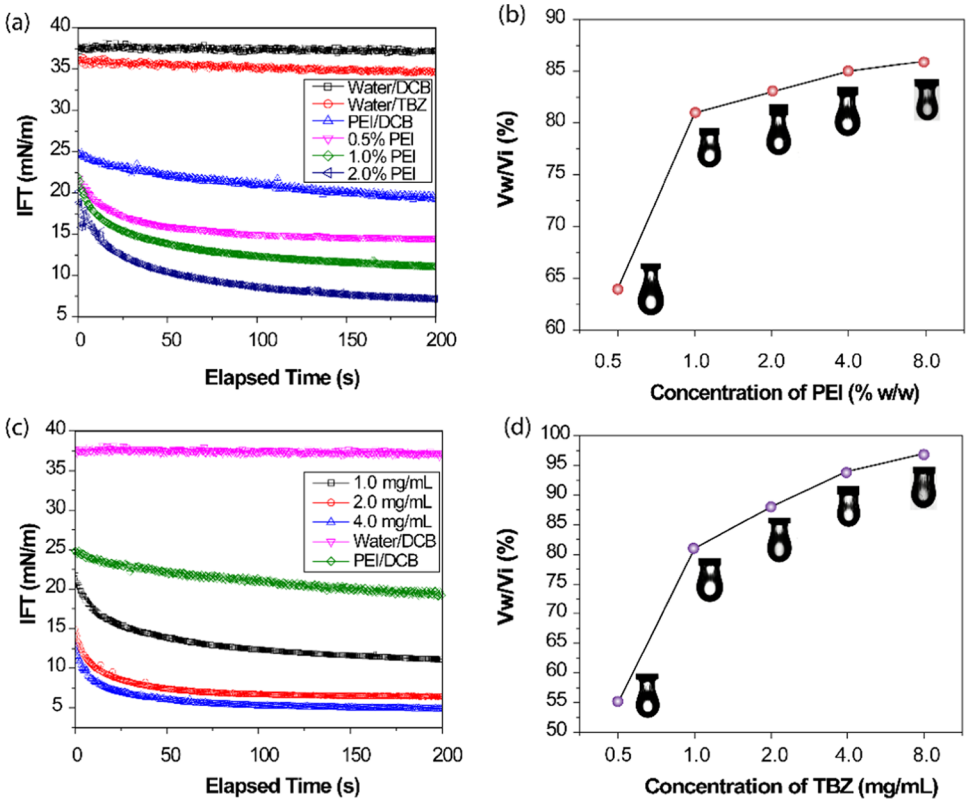

Figure 2. (a) Time evolution of interfacial tension and (b) surface coverage with TBZ (1.0 mg/mL) and varying PEI concentrations. (c) Time evolution of interfacial tension and (d) surface coverage with PEI (1% w/w) and varying TBZ concentrations.

interface. Later, the nanoscopic structure of the film was investigated by AFM (see the Supporting Information, Figure S11), and the micrograph showed the formation of closely packed aggregates with the size ranging from 150 to 200 nm, and the height was 20 nm. After analyzing the assembly of PEI/TBZ at the interface, we were curious to investigate the

https://doi.org/10.1021/acs.langmuir.2c00725
Langmuir 2022, 38, 8296−8303

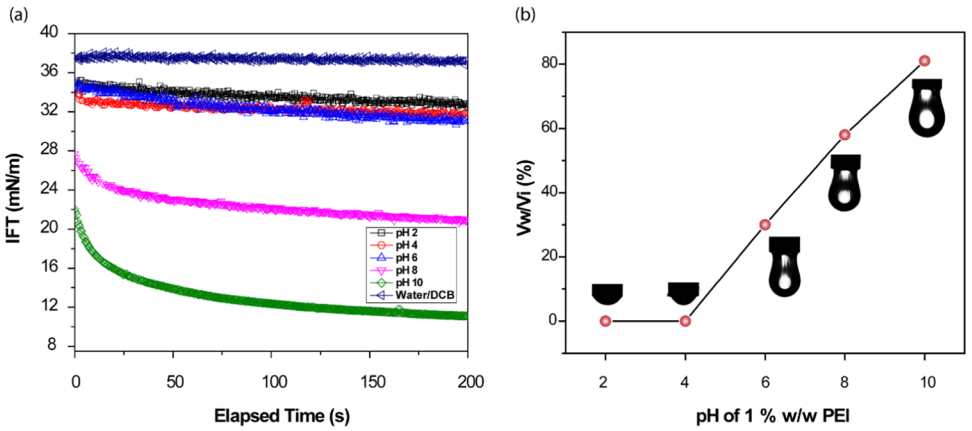

Figure 3. (a) Time evolution of interfacial tension and (b) surface coverage with TBZ (1.0 mg/mL) and varying pH values of PEI (1% w/w).

assembly of two other aldehyde variants, DBZ and SBZ, with PEI. The equilibrium interfacial tension of the PEI/DBZ system was very similar to that of the TBZ system, probably due to the similar crosslinking ability of bi- and trifunctional aldehyde groups with PEI at the interface. In the presence of SBZ, the equilibrium interfacial tension was higher (14 mN/m) compared to the previous analogues because of the presence of single aldehyde functionality in SBZ.

Anisotropic compartmentalization of the liquid−liquid interface provides ample opportunity to fabricate microbots and smart-release systems.[33,34] The isotropic liquid droplet can be compressed beyond its critical surface coverage, which can lead to interfacial jamming, i.e., nonejection of assemblies from the interface. We anticipated that the jamming of imine-based assemblies at the interface would lock the droplet in a nonequilibrium shape, paving the way to create an anisotropic liquid compartment. It was initially demonstrated through PEI (1% w/w aq. solution) and TBZ (1.0 mg/mL in DCB) using a pendant drop tensiometer. A TBZ droplet (1.0 mg/mL) was injected into the cuvette filled with PEI solution and was allowed to react for 3 min. Upon decreasing the volume of the oil droplet, wrinkling of the interfacial film was observed, and it was a clear indication of interfacial jamming of imine-mediated assembly. As shown in Figure 1a,b, the shape of the droplet was distorted when extracting the oil volume but recovered to its original shape upon reinjecting the initial volume (see also the Supporting Information, SV1). This extraction−reinjection process can be repeated several times without disrupting the interfacial film, suggesting the robustness of the interfacial film. We further examined the time evolution of IFT (Figure 1c) and packing density of imine assembly at the interface by decreasing the initial volume V_i and comparing this to the volume measured when wrinkling was first observed, V_w. From the V_w/V_i ratio, the compression ratio to jam the interfacial assembly can be determined, and the fraction of the interface occupied by the imine assembly can be estimated. Figure 1d shows how the ratio of V_w/V_i changes as a function of the aldehyde variants after aging the assembly for only 3 min. TBZ and DBZ showed similar surface coverage (~80%), whereas SBZ showed a surface coverage of 56% only. It is evident from this observation that as the number of aldehyde functionalities increases, the extended crosslinking between the imine assemblies is quickly achieved to attain the nonequilibrium shape via interfacial jamming.

To gain a deeper insight into how the concentration of PEI and aldehyde affects the interfacial assembly as well as jamming at the interface, we studied the PEI/TBZ pair by altering the concentration of one constituent at a time. At a fixed concentration of TBZ (1.0 mg/mL), the equilibrium interfacial tension was 14.2 mN/m with 0.5% w/w PEI and was gradually reduced to 7.1 mN/m with 2% w/w PEI (Figure 2a). The expected outcome inferred that with increasing PEI concentration, the population of imine assemblies at the interface increased, thus lowering the interfacial tension. The effect was more prominent when the droplet volume was reduced to form a jammed assembly. The initial V_w/V_i was 64% when the concentration of PEI was 0.5% w/w. As the concentration of PEI was increased to 2% w/w, the value of V_w/V_i was maximum up to 83%, as shown in Figure 2b. At even higher concentrations of PEI, i.e., with 4 and 8% w/w, the value of V_w/V_i was 85 and 86%, respectively. We observed a similar trend by varying the concentration of TBZ while PEI concentration was kept constant at 1% w/w. It was found that the equilibrium interfacial tension decreased from 11 to 4.9 mN/m when the TBZ concentration ranged from 1.0 to 4.0 mg/mL (Figure 2c). We also studied the V_w/V_i from the lowest (0.5 mg/mL) to the highest (8.0 mg/mL) concentration of TBZ, and it was found to increase from 55 to 96%, respectively. (Figure 2d; see also the Supporting Information, SV2)

The branched PEI bears a great number of primary amine groups, and the charge density of this polymer can be modulated by changing the pH of the solution. In an acidic pH (<4), the polymer exists in its maximum protonated counterpart and is thus unable to undergo a nucleophilic reaction with an aldehyde group. On the other hand, at a basic pH (>9), the primary amines are mostly in the $-NH_2$ form, and they can form an imine bond by reacting with an aldehyde. The interfacial assembly of PEI and TBZ was investigated as a function of the pH value of the aqueous phase, ranging from pH 2 to 10. It was observed that the equilibrium interfacial tension increased as the pH of the aqueous PEI solution was increased. As shown in Figure 3a, the equilibrium interfacial tension was found to be 32.9 and 31.8 mN/m at pH 2 and pH 4, respectively. At such an acidic pH, when the interfacial area was reduced, no jamming was observed at the interface, as shown in the Supporting Video SV3. This suggested that the imine bond formation between PEI and TBZ at a lower pH was futile. Contrarily, at a higher pH range, the equilibrium interfacial tension started to drop, i.e., at pH 6, the interfacial tension was 30.7 mN/m, and wrinkles appeared with a surface coverage of 30%, confirming imine formation at the interface.

https://doi.org/10.1021/acs.langmuir.2c00725
Langmuir 2022, 38, 8296−8303

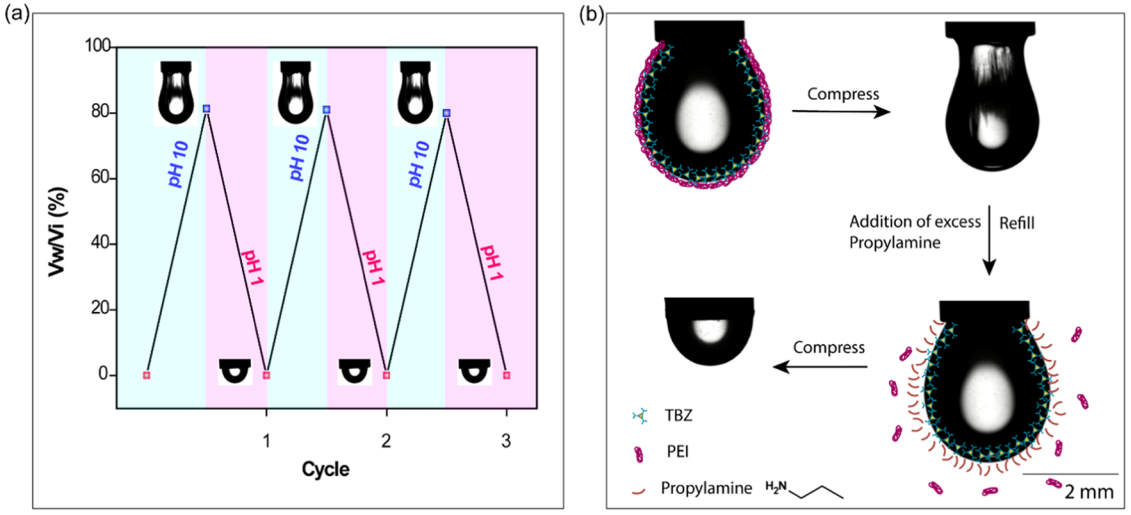

Figure 4. Representation of (a) pH-dependent reversible assembly and disassembly of a droplet by adding an acid/base. Surface coverage was noted after aging the droplet for 200 s. (b) Imine exchange at the PEI/TBZ cross-linked interface with a primary amine, propylamine (concentrations were 1% w/w for PEI, 1.0 mg/mL for TBZ, 5% w/w for propylamine).

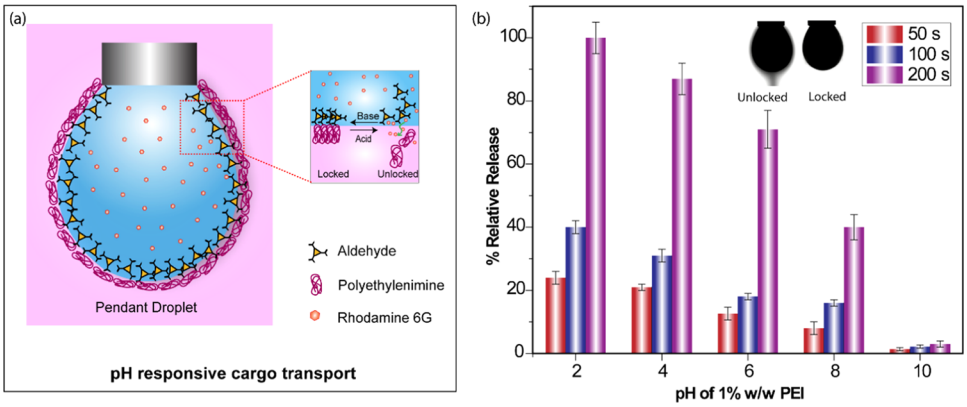

Figure 5. (a) Schematic representation of the PEI/TBZ assembly for cargo transport (PEI, 1% w/w; TBZ, 1.0 mg/mL). (b) Relative release of Rh6G at different pH values of PEI for 50, 100, and 200 s, taken at 530 nm. The inset picture shows the unlocked and locked states of the droplet.

At pH 8, the equilibrium interfacial tension was found to be 20.1 mN/m with a surface coverage of 58% (Figure 3b). Finally, at pH 10, the equilibrium IFT was the lowest, i.e., 11.1 mN/m, indicating maximum interfacial activity with a surface coverage of 81% (Supplementary Video SV4). We also performed control experiments with DCB and PEI (1% w/w) solutions at a pH range of 2−10 and confirmed that only PEI could not contribute to the interfacial jamming. (See Supporting Information Figure S12 for IFT data.)

After studying the pH-dependent interfacial activity of the TBZ and PEI pair, we explored the reversible and dynamic nature of imine bond formation that would pave the way for numerous stimuli-responsive systems. For this study, the pH of the system was switched from acidic (pH 1) to basic (pH 10), and the resultant interfacial jamming to unjamming transition was noted. Initially, the experiment was conducted at an acidic pH, and once the equilibrium interfacial tension was attained, the volume of the droplet was reduced to examine the wrinkle formation. As previously observed, at an acidic pH, the imine bond formation did not occur, and no wrinkles were observed. Next, the pH of the aqueous solution was adjusted to pH 10 by adding NaOH to the solution. The interfacial jamming was observed, and the surface coverage was 81% as observed earlier. When HCl was added to alter the pH of the system to pH 1, the preformed wrinkles disappeared. Even after compressing the droplet to its minimum volume, there was no evidence of wrinkle formation. This cycle was repeated multiple times to corroborate the reversible and robust nature of the interfacial film, as shown in Figure 4a.

The dynamic nature of the imine bond formation was verified by introducing a competing primary amine that went through an amine exchange process at the interface. For this study, the PEI and TBZ pair was used to form an imine-mediated crosslinking at the interface. The wrinkle was observed upon compressing the droplet volume, confirming the imine bond formation as seen in earlier experiments. At this point, an excess amount of propylamine, a monofunctional amine, was added to the aqueous solution of the droplet. We anticipated that the amine exchange would lead to the formation of a new imine bond with TBZ, and it would replace the existing PEI-based assemblies. As a result, the polyamine-based crosslinking at the interface will disappear. After 5 min of aging the droplet with propylamine, the wrinkles disappeared, suggesting the formation of a new imine bond at the interface, as shown in Figure 4b (see also the Supporting Information, SV5). To confirm the same, we performed a control experiment where the TBZ/propylamine pair was used to form the imine bond at the interface. There was no

https://doi.org/10.1021/acs.langmuir.2c00725
Langmuir 2022, 38, 8296−8303

interfacial crosslinking in this case (see the Supporting Information, SV6). It was further confirmed by measuring the interfacial tension of the TBZ/propylamine pair. The equilibrium interfacial tension value was 17.3 mN/m, which indicated that the pair was not interfacially active as compared to TBZ/PEI (see the Supporting Information, Figure S13).

Mimicking the selective permeability of cell membranes has always been a challenge.[35] Thus, the imitation of selective transport across the membrane has attracted immense interest in recent days. Herein, we intend to investigate the molecular transport across the interfacially structured PEI/TBZ membrane. For this study, we used Rhodamine 6G (Rh6G) as a tracer dye owing to its ease of partitioning and detection. The Rh6G dye was initially dissolved in DCB along with TBZ, keeping the concentration at 1.0 mg/mL. The oil drop was then suspended in the aqueous solution of PEI. The schematic of the process is shown in Figure 5a. This study was carried out over a wide range of pH values as described earlier. The dye slowly diffused into the water phase, and the amount of Rh6G released was quantified by measuring the absorbance at 530 nm with UV−vis spectrometry. We performed this experiment at a time point of 200 s, where we collected the solutions and measured UV absorbance. It was observed that the diffusion of Rh6G decreased with an increase in the pH. This observation corroborated the pH-responsive wrinkling and surface coverage of the PEI/TBZ interfacial assembly. At pH 10, the maximum crosslinking through the imine bond occurred at the interface. Thus the diffusion of dye molecules through this interfacial membrane was difficult (locked state, 3% release). The opposite scenario was observed at pH 2 (unlocked state, 100% release), where interfacial crosslinking was negligible, and the dye release was maximum. We also measured the release of dye at various pH values, which were found to be 87% at pH 4, 71% at pH 6, and 40% at pH 8. We also studied the release at different time points of 50 and 100 s, respectively. We observed that the release increased linearly from 50 to 200 s and decreased from pH 2 to pH 10, as shown in Figure 5b. It is quite evident from the observation that the imine-based interfacial assemblies provided a selective, stimuli-responsive transport across the boundary.

3. CONCLUSIONS

In this work, we demonstrated the formation of a dynamic covalent imine bond at the oil−water interface, and a nonequilibrium shape of the oil-in-water droplet was created via interfacial jamming. We described the varied nature of interfacial assembly depending on the concentration of the reactants, degree of crosslinking, and pH of the surrounding environment. We made judicious use of the pH dependency of the Schiff base reaction to shift the equilibrium, which resulted in reversible toggling of jamming to unjamming interfacial assembly. We further demonstrated triggered cargo release by changing the pH of the system. Overall, our results offer great applications in the field of dynamic covalent assemblies at the interface, structuring liquid droplets and smart membranes.

4. EXPERIMENTAL SECTION

4.1. Materials. Polyethylenimine (PEI), branched with an average M_w of 25,000, 2,4,6-trichloro-1,3,5-triazine, 4-hydroxy benzaldehyde, and tetrabutylammonium bromide were purchased from Sigma-Aldrich. Dichloromethane and methanol were purchased from Merck. 1,2-Dichlorobenzene was purchased from TCI. 4-((4,6-Dimethoxy-1,3,5-triazin-2-yl)oxy)benzaldehyde, 4,4′-((6-methoxy-1,3,5-triazine-2,4-diyl)bis(oxy))dibenzaldehyde, and 4,4′,4″-((1,3,5-triazine-2,4,6-triyl)tris(oxy))tribenzaldehyde were synthesized as per the literature. Millipore water (18.2 MΩ·cm at 25 °C) was used in all interfacial tension measurements.

4.2. Characterization. The dynamic interfacial tension (γ) was analyzed with a tensiometer (DSA25 Drop Shape Analyzer, KRÜSS GmbH) using a pendant-drop method, where the evolution of γ with time was recorded after the oil phase (1,2-dichlorobenzene) was slowly injected into the aqueous phase. The deformation and wrinkling behavior were recorded as images or videos with a digital camera. Confirmation of imine bond formation was carried out using the Thermo Scientific Nicolet iS20 FTIR instrument. The surface morphology of the interfacial film was studied by atomic force microscopy (Bruker Multimode 8 system). UV absorption spectra were measured on a SHIMADZU UV-2600 spectrophotometer. NMR spectra were recorded on a Bruker Avance 400 MHz NMR spectrometer.

■ ASSOCIATED CONTENT

Supporting Information

The Supporting Information is available free of charge at https://pubs.acs.org/doi/10.1021/acs.langmuir.2c00725.

General methods and characterization; synthesis and characterization of aldehydes; IR and AFM of the interfacial film; imine exchange at the interface; and supporting videos regarding the morphology evolution of droplets under various conditions (PDF)

Morphology evolution of a droplet under compression (TBZ 1 mg/mL, PEI 1% w/w at pH 10) with the extraction and reinjection process without any breakage (SV1) (MP4)

Morphology evolution of a droplet under compression (4 mg/mL TBZ, 1% w/w PEI at pH 10) (SV2) (MP4)

Morphology evolution of a droplet under compression (1 mg/mL TBZ, 1% w/w PEI at pH 2) (SV3) (MP4)

Morphology evolution of a droplet under compression (1.0 mg/mL TBZ, 1% w/w PEI at pH 10) (SV4) (MP4)

Morphology evolution of a droplet under compression (1.0 mg/mL TBZ, 1% w/w propylamine) (SV5) (MP4)

Morphology evolution of a droplet under compression during imine exchange (1.0 mg/mL TBZ, 1% w/w PEI, 5% w/w propylamine) (SV6) (MP4)

■ AUTHOR INFORMATION

Corresponding Author

Debabrata Patra − *Institute of Nano Science and Technology, Mohali 140306 Punjab, India*; orcid.org/0000-0003-4099-7880; Email: patra@inst.ac.in

Authors

Chinmayee Agashe − *Institute of Nano Science and Technology, Mohali 140306 Punjab, India*

Rohit Varshney − *Institute of Nano Science and Technology, Mohali 140306 Punjab, India*

Rekha Sangwan − *Institute of Nano Science and Technology, Mohali 140306 Punjab, India*

Arshdeep K. Gill − *Institute of Nano Science and Technology, Mohali 140306 Punjab, India*

Mujeeb Alam − *Institute of Nano Science and Technology, Mohali 140306 Punjab, India*

Complete contact information is available at: https://pubs.acs.org/10.1021/acs.langmuir.2c00725

https://doi.org/10.1021/acs.langmuir.2c00725
Langmuir 2022, 38, 8296−8303

Author Contributions

The manuscript was written through contributions of all authors. All authors have given approval to the final version of the manuscript.

Funding

The work was financially supported by SERB-DST (ECR/2017/000442).

Notes

The authors declare no competing financial interest.

■ ACKNOWLEDGMENTS

D.P. acknowledges the financial support by SERB-DST (ECR/2017/000442).

■ ABBREVIATIONS

PEI, polyethyleneimine; SBZ, 4-((4,6-dimethoxy-1,3,5-triazin-2-yl)oxy)benzaldehyde; DBZ, 4,4′-((6-methoxy-1,3,5-triazine-2,4-diyl)bis(oxy))dibenzaldehyde; TBZ, 4,4′,4″-((1,3,5-triazine-2,4,6-triyl)tris(oxy))tribenzaldehyde; DCB, 1,2-dichlorobenzene; Rh-6G, Rhodamine 6G

■ REFERENCES

(1) Xie, G.; Forth, J.; Zhu, S.; Helms, B. A.; Ashby, P. D.; Shum, H. C.; Russell, T. P. Hanging droplets from liquid surfaces. *Proc. Natl. Acad. Sci. U.S.A.* **2020**, *117*, 8360−8365.

(2) Xie, G.; Forth, J.; Chai, Y.; Ashby, P. D.; Helms, B. A.; Russell, T. P. Compartmentalized, all-aqueous flow-through-coordinated reaction systems. *Chem* **2019**, *5*, 2678−2690.

(3) Cao, Q.; Amini, S.; Kumru, B.; Schmidt, B. V. K. J. Molding and Encoding Carbon Nitride-Containing Edible Oil Liquid Objects via Interfacial Toughening in Waterborne Systems. *ACS Appl. Mater. Interfaces* **2021**, *13*, 4643−4651.

(4) Forth, J.; Liu, X.; Hasnain, J.; Toor, A.; Miszta, K.; Shi, S.; Geissler, P. L.; Emrick, T.; Helms, B. A.; Russell, T. P. Reconfigurable printed liquids. *Adv. Mater.* **2018**, *30*, No. 1707603.

(5) Feng, W.; Chai, Y.; Forth, J.; Ashby, P. D.; Russell, T. P.; Helms, B. A. Harnessing liquid-in-liquid printing and micropatterned substrates to fabricate 3-dimensional all-liquid fluidic devices. *Nat. commun* **2019**, *10*, No. 1095.

(6) Jaeger, H. M. Celebrating soft matter's 10th anniversary: Toward jamming by design. *Soft matter* **2015**, *11*, 12−27.

(7) Forth, J.; Kim, P. Y.; Xie, G.; Liu, X.; Helms, B. A.; Russell, T. P. Building reconfigurable devices using complex liquid−fluid interfaces. *Adv. mater.* **2019**, *31*, No. 1806370.

(8) Shi, S.; Russell, T. P. Nanoparticle assembly at liquid−liquid interfaces: From the nanoscale to mesoscale. *Adv. Mater.* **2018**, *30*, No. 1800714.

(9) Patra, D.; Sanyal, A.; Rotello, V. M. Colloidal Microcapsules: Self-Assembly of Nanoparticles at the Liquid−Liquid Interface. *Chem. Asian J.* **2010**, *5*, 2442−2453.

(10) Hou, H.; Li, J.; Li, X.; Forth, J.; Yin, J.; Jiang, X.; Helms, B. A.; Russell, T. P. Interfacial Activity of Amine-Functionalized Polyhedral Oligomeric Silsesquioxanes (POSS): A Simple Strategy To Structure Liquids. *Angew. Chem.* **2019**, *131*, 10248−10253.

(11) Shi, S.; Liu, X.; Li, Y.; Wu, X.; Wang, D.; Forth, J.; Russell, T. P. Liquid letters. *Adv. Mater.* **2018**, *30*, No. 1705800.

(12) Xu, R.; Liu, T.; Sun, H.; Wang, B.; Shi, S.; Russell, T. P. Interfacial assembly and jamming of polyelectrolyte surfactants: A simple route to print liquids in low-viscosity solution. *ACS Appl. Mater. Interfaces* **2020**, *12*, 18116−18122.

(13) Varshney, R.; Agashe, C.; Gill, A. K.; Alam, M.; Joseph, R.; Patra, D. Modulation of liquid structure and controlling molecular diffusion using supramolecular constructs. *Chem.Commun.* **2021**, *57*, 10604−10607.

(14) Luo, J.; Zeng, M.; Peng, B.; Tang, Y.; Zhang, L.; Wang, P.; He, L.; Huang, D.; Wang, L.; Wang, X.; et al. Electrostatic-driven dynamic jamming of 2D nanoparticles at interfaces for controlled molecular diffusion. *Angew. Chem.* **2018**, *130*, 11926−11931.

(15) Chai, Y.; Hasnain, J.; Bahl, K.; Wong, M.; Li, D.; Geissler, P.; Kim, P. Y.; Jiang, Y.; Gu, P.; Li, S.; et al. Direct observation of nanoparticle-surfactant assembly and jamming at the water-oil interface. *Sci. Adv.* **2020**, *6*, No. eabb8675.

(16) Sun, S.; Xie, C.; Chen, J.; Yang, Y.; Li, H.; Russell, T. P.; Shi, S. Responsive Interfacial Assemblies Based on Charge-Transfer Interactions. *Angew. Chem.* **2021**, *133*, 26567−26571.

(17) Sun, H.; Li, L.; Russell, T. P.; Shi, S. Photoresponsive Structured Liquids Enabled by Molecular Recognition at Liquid−Liquid Interfaces. *J. Am. Chem. Soc.* **2020**, *142*, 8591−8595.

(18) Belowich, M. E.; Stoddart, J. F. Dynamic imine chemistry. *Chem. Soc. Rev.* **2012**, *41*, 2003−2024.

(19) Acharyya, K.; Mukherjee, P. S. Organic imine cages: molecular marriage and applications. *Angew. Chem.* **2019**, *131*, 8732−8745.

(20) Zentner, C. A.; Anson, F.; Thayumanavan, S.; Swager, T. M. Dynamic imine chemistry at complex double emulsion interfaces. *J. Am. Chem. Soc.* **2019**, *141*, 18048−18055.

(21) Chen, H.; Zhao, R.; Hu, J.; Wei, Z.; McClements, D. J.; Liu, S.; Li, B.; Li, Y. One-step dynamic imine chemistry for preparation of chitosan-stabilized emulsions using a natural aldehyde: acid trigger mechanism and regulation and gastric delivery. *J. Agric. Food Chem.* **2020**, *68*, 5412−5425.

(22) Ji, Y.; Mu, W.; Wu, H.; Qiao, Y. Directing Transition of Synthetic Protocell Models via Physicochemical Cues-Triggered Interfacial Dynamic Covalent Chemistry. *Adv. Sci.* **2021**, *8*, No. 2101187.

(23) Xin, Y.; Yuan, J. Schiff's base as a stimuli-responsive linker in polymer chemistry. *Polym. Chem.* **2012**, *3*, 3045−3055.

(24) Halder, A.; Karak, S.; Addicoat, M.; Bera, S.; Chakraborty, A.; Kunjattu, S. H.; Pachfule, P.; Heine, T.; Banerjee, R. Ultrastable imine-based covalent organic frameworks for sulfuric acid recovery: an effect of interlayer hydrogen bonding. *Angew. Chem., Int. Ed.* **2018**, *57*, 5797−5802.

(25) Das, G.; Shinde, D. B.; Kandambeth, S.; Biswal, B. P.; Banerjee, R. Mechanosynthesis of imine, *β*-ketoenamine, and hydrogen-bonded imine-linked covalent organic frameworks using liquid-assisted grinding. *Chem. Commun.* **2014**, *50*, 12615−12618.

(26) Greb, L.; Lehn, J.-M. Light-driven molecular motors: imines as four-step or two-step unidirectional rotors. *J. Am. Chem. Soc.* **2014**, *136*, 13114−13117.

(27) Minkenberg, C. B.; Florusse, L.; Eelkema, R.; Koper, G. J.; van Esch, J. H. Triggered self-assembly of simple dynamic covalent surfactants. *J. Am. Chem. Soc.* **2009**, *131*, 11274−11275.

(28) Minkenberg, C. B.; Li, F.; van Rijn, P.; Florusse, L.; Boekhoven, J.; Stuart, M. C.; Koper, G. J.; Eelkema, R.; van Esch, J. H. Responsive vesicles from dynamic covalent surfactants. *Angew. Chem., Int. Ed.* **2011**, *50*, 3421−3424.

(29) ávan Esch, J. H. Dynamic covalent assembly of stimuli responsive vesicle gels. *Chem.Commun.* **2012**, *48*, 9837−9839.

(30) Shome, A.; Das, A.; Rawat, N.; Rather, A. M.; Manna, U. Reduction of imine-based cross-linkages to achieve sustainable underwater superoleophobicity that performs under challenging conditions. *J. Mater. Chem. A* **2020**, *8*, 15148−15156.

(31) Yang, M.; Sun, Y.; Chen, G.; Wang, G.; Lin, S.; Sun, Z. Preparation of a self-healing silicone coating for inhibiting adhesion of benthic diatoms. *Mater. Lett.* **2020**, *268*, No. 127496.

(32) Vácha, R.; Rick, S. W.; Jungwirth, P.; de Beer, A. G.; de Aguiar, H. B.; Samson, J.-S.; Roke, S. The orientation and charge of water at the hydrophobic oil droplet−water interface. *J. Am. Chem. Soc.* **2011**, *133*, 10204−10210.

(33) Wang, H.; Zhao, Z.; Liu, Y.; Shao, C.; Bian, F.; Zhao, Y. Biomimetic enzyme cascade reaction system in microfluidic electrospray microcapsules. *Sci. Adv.* **2018**, *4*, No. eaat2816.

(34) Fischlechner, M.; Schaerli, Y.; Mohamed, M. F.; Patil, S.; Abell, C.; Hollfelder, F. Evolution of enzyme catalysts caged in biomimetic gel-shell beads. *Nat. Chem.* **2014**, *6*, 791−796.

https://doi.org/10.1021/acs.langmuir.2c00725
Langmuir 2022, 38, 8296−8303

(35) Yang, N. J.; Hinner, M. J. Getting across the cell membrane: an overview for small molecules, peptides, and proteins. *Methods Mol Biol.* **2015**, *1266*, 29−53.

https://doi.org/10.1021/acs.langmuir.2c00725
Langmuir 2022, 38, 8296−8303